Pseudo-steady rates of crystal nucleation in suspensions of charged colloidal particles

2003 J. Phys.: Condens. Matter 15 1531

(http://iopscience.iop.org/0953-8984/15/10/303)

INSTITUTE OF PHYSICS PUBLISHING JOURNAL OF PHYSICS: CONDENSED MATTER

J. Phys.: Condens. Matter **15** (2003) 1531–1552 PII: S0953-8984(03)57131-4

Pseudo-steady rates of crystal nucleation in suspensions of charged colloidal particles

Narendra M Dixit and Charles F Zukoski[1]

Department of Chemical and Biomolecular Engineering, University of Illinois at Urbana-Champaign 114, Roger Adams Laboratory, 600 S Mathews Avenue, Urbana, IL 61801, USA

E-mail: czukoski@uiuc.edu

Received 4 December 2002
Published 3 March 2003
Online at stacks.iop.org/JPhysCM/15/1531

Abstract

We develop an analytical model to describe crystal nucleation in suspensions of charged colloidal particles. The particles are assumed to interact with a repulsive hard-core Yukawa potential. The thermodynamic properties of the suspensions are determined by mapping onto an effective hard-sphere system using perturbation theory. Hydrodynamic effects are calculated by approximating particle interactions with the excluded shell potential. The rates of particle aggregation and dissociation from cluster surfaces in supersaturated suspensions are determined by solving the diffusion and Smoluchowski equations, respectively, which allow the calculation of pseudo-steady rates of crystal nucleation. By decoupling thermodynamic and hydrodynamic effects, we find intriguing non-monotonic dependencies of the nucleation rate on the strength and the range of particle repulsions. In particular, we find that the rate at any effective hard-sphere volume fraction can be lower than that of the hard-sphere system at that volume fraction. Model calculations are in qualitative agreement with recent experiments and semi-quantitative agreement with simulations.

1. Introduction

At a fixed temperature, increasing the concentration of particles in a suspension of uniformly charged colloidal particles results in a crystallization transition analogous to the entropic order–disorder transition in hard-sphere suspensions [1–8]. While the hard-sphere case is well understood, a consistent description of the crystallization of charged sphere suspensions, applicable over wide ranges of particle volume fractions and strengths and ranges of particle repulsions, is yet to be developed. When particles experience short-range repulsions, the

[1] Author to whom any correspondence should be addressed.

0953-8984/03/101531+22$30.00

equilibrium thermodynamics of this crystallization transition is captured by theories developed for hard-sphere suspensions by treating the charged particles as effective hard spheres of larger sizes [1]. Encouraged by this generalization, attempts have been made to understand the kinetics of crystallization in charged colloidal suspensions using the effective hard-sphere description [9–11]. Unlike crystal nucleation in hard-sphere suspensions, which is extremely well studied [9, 10, 12–15], crystal nucleation in charged colloidal suspensions remains poorly explored, leaving limited studies to rigorously test the effective hard-sphere description. Recent experiments and simulations reveal that significant differences exist between the kinetics of crystallization in hard-sphere and charged-sphere suspensions [9–11, 16, 17].

Chief among the differences between hard-sphere and charged-sphere suspensions is the dependence of the nucleation rate, J, defined as the rate at which stable crystals form in a unit volume of the suspension, on the particle volume fraction, ϕ. For hard-sphere suspensions, J passes through a maximum upon increasing ϕ above the solubility boundary, $\phi_s = 0.495$ [9, 14]. For small increases in ϕ above ϕ_s, the thermodynamic driving force for crystallization increases, resulting in an increase in J. For larger increases, however, the suspensions become increasingly crowded. As the random close packing volume fraction for hard-spheres, $\phi_{cp} = 0.64$, is approached, the particle mobility is drastically reduced causing J to decrease. In fact, a glass transition is observed at $\phi \sim 0.58$, where particle motion is arrested over any measurable timescale [18]. As a result of these competing influences, a maximum in J occurs at $\phi \sim 0.55$ for hard-sphere suspensions. For charged colloidal suspensions, in the limited studies conducted so far, the location of this maximum is found to depend sensitively on the strength and the range of the repulsions, and is often not observed [9–11, 16, 17].

A plausible explanation for this difference is that for charged systems, ϕ_s can be orders of magnitude lower than 0.495 [1–8]. As a result, hydrodynamic effects due to particle crowding do not influence crystal nucleation except for very large increases in ϕ above ϕ_s. J therefore increases monotonically with ϕ over a wider range of particle concentrations. This qualitative difference is also manifested in the different dependencies of other measures of nucleation kinetics, such as induction times and crystal growth velocities, on the particle volume fraction observed in hard-sphere and charged-sphere suspensions [9–11, 16, 17]. At the same time, in the effective hard-sphere model, the particles look thermodynamically larger than the core size due to the electrostatic repulsions. Thus as the effective hard-sphere volume fraction approaches 0.58, glasses are expected to form independent of hydrodynamic interactions. Indeed, glasses are observed in charged colloidal suspensions at values of ϕ comparable to ϕ_s when $\phi_s \ll 1$ [2, 16]. Nucleation is suppressed under these conditions, although the maximum in J may not occur until much later than an effective volume fraction of $\sim$0.55. This suggests that a subtle interplay of hydrodynamic and thermodynamic effects underlies phase transitions, and particularly their kinetics, in charged systems. Here, we explore the role of hydrodynamic and thermodynamic effects in the kinetics of crystal nucleation in charged colloidal suspensions.

In an attempt to formalize the differences between hard-sphere and charged-sphere suspensions, Russel [10] proposed an adaptation of classical nucleation theory to predict crystal nucleation and growth rates in these suspensions. In this adaptation, approximate expressions for the self-diffusivity of particles in dense suspensions are employed to describe the motion of hard-sphere particles during crystallization, whereas the Stokes–Einstein diffusivity, applicable in the dilute limit, is assumed to describe the motion of charged particles. Model predictions of growth rates capture the qualitative distinctions between hard-sphere and charged-sphere systems, but quantitative comparisons require adjustable parameters.

Auer and Frenkel [19] recently conducted simulation studies using the Yukawa potential to describe pair interactions. The Yukawa potential is a standard model to describe

weak electrostatic repulsions between charged particles in suspension. Again, classical nucleation theory with an approximate expression for the particle self-diffusivity to account for hydrodynamic interactions is employed to determine steady state nucleation rates. Interestingly, depending on the strength and the range of the repulsive interactions, drastically different nucleation rates are predicted at similar supersaturations. In particular, a non-monotonic dependence on the range of the repulsion is observed: at any supersaturation, the nucleation rate first increases and then decreases as the range is increased. In all cases, the rates are consistently higher than those for hard-sphere suspensions.

The Yukawa system is known to display solid–solid (bcc–fcc) transitions as, depending on the strength and the range of particle interactions, either the bcc or the fcc structure is the thermodynamically stable solid state [2, 7, 8]. Interestingly, however, the simulations of Auer and Frenkel reveal that regardless of the stable state, the initial crystal nuclei always have a bcc structure. Auer and Frenkel compare their estimates of nucleation rates to the experiments of Gasser *et al* [20] and find significant discrepancies. They attribute the discrepancies to the density dependence of particle interactions not accounted for in their simulations.

The discrepancies between model predictions and experiments and between simulations and experiments leave unclear the ability of classical nucleation theory to describe nucleation kinetics in charged colloidal suspensions. Motivated by the limitations of classical theories, we recently developed a kinetic approach for calculating nucleation rates in hard-sphere suspensions [12, 13]. In this approach, particle gradient diffusivity rather than self-diffusivity is assumed to dictate particle motion during crystallization. Crystal nucleation is described as the result of a competition between two processes: the aggregation of single particles onto, and the dissociation of single particles from, cluster surfaces. Based on descriptions of the rates of these processes, population balance is used to determine the time evolution of the cluster size distribution during crystallization. This allows calculation of the quantities measured in light scattering experiments commonly employed to probe the kinetics of colloidal crystallization. Model calculations are in excellent agreement with experimental estimates of nucleation rates, induction times, and crystal growth rates in hard-sphere suspensions.

In this paper, we extend the kinetic approach to charged colloidal suspensions. Key to this adaptation is to account correctly for the distinct ϕ dependencies of the thermodynamic and hydrodynamic interactions that affect crystal nucleation kinetics in these suspensions. Drawing from previous studies [1], we argue that the effective hard-sphere volume fraction, ϕ_{eff}, determines the thermodynamic driving force for crystallization, whereas hydrodynamic effects depend on the actual particle volume fraction, ϕ. Assuming particles interact with the Yukawa potential, we determine ϕ_{eff} using the perturbation theory developed by Kang *et al* [21]. The thermodynamic driving force for crystallization is then obtained from theories for hard-sphere suspensions. In doing so, we ignore the subtle differences arising from the variable structure of the stable solid state, i.e., bcc or fcc. This limits our studies to cases where the range of the repulsion is relatively small compared to the particle size, as is often the case where colloidal crystals are observed experimentally [20]. To quantify hydrodynamic effects, the gradient diffusivity of the particles is determined as a function of ϕ by representing particle interactions with an excluded shell potential [1]. The rates of particle aggregation and dissociation processes are then determined as for hard-sphere suspensions. This allows the calculation of pseudo-steady-state rates of crystal nucleation in charged colloidal suspensions.

These calculations suggest that intriguing effects arise due to the decoupling of thermodynamic and hydrodynamic effects in charged systems. In agreement with the simulations of Auer and Frenkel [19], we find that drastically different rates result at identical supersaturations as the strength and the range of particle interactions are varied. In addition, we find non-monotonic dependencies of the rates on both the strength and the range of particle

interactions. In contrast to the simulations, however, we find that the rates can be lower than those observed for hard-sphere systems. This we attribute to the diminishing near field hydrodynamic interactions as the particles become more repulsive, which allows particles on cluster surfaces to dissociate at enhanced rates. Finally, we find that the maximum in the nucleation rate observed for hard-sphere suspensions gradually shifts to higher ϕ_{eff} as the particles become more repulsive, explaining why in many of the reported observations the maximum is missed. Comparisons indicate that model predictions are in qualitative agreement with experiments and semi-quantitative agreement with simulations.

The paper is organized as follows. In section 2, we outline the perturbation theory of Kang *et al* for calculating the effective hard-sphere size for repulsive particles and describe the resulting equilibrium thermodynamics of charged colloidal suspensions. In section 3, we develop our description of the kinetics of crystal nucleation in these suspensions. We present model calculations of nucleation rates in section 4 and compare them with experiments and simulations in section 5. Our conclusions are summarized in section 6.

2. Equilibrium thermodynamics

We consider a suspension of uniformly charged colloidal particles of hard-core radii a occupying a volume fraction ϕ. The pair interactions of the particles in suspension are well approximated by the hard-core Yukawa potential [1–8]:

$$\frac{V(r)}{kT} = \begin{cases} \infty & r \leqslant 2a \\ \dfrac{\varepsilon}{kT}\dfrac{\exp(-\kappa(r/2a-1))}{r/2a} & r > 2a \end{cases} \tag{1}$$

where r is the centre-to-centre separation of a pair of particles, ε is the strength of the repulsive interactions, κ is the inverse screening length, and kT is the product of Boltzmann's constant and absolute temperature. ε and κ depend on the charge on the particles (or their surface potential), the particle size, and the concentration of ions in the suspension, and in less well understood ways on the particle concentration. In the limit of very short-range, weak repulsions, where $\varepsilon \to 0$ and $\kappa \to \infty$, the Yukawa potential reduces to the hard-sphere potential.

Solution thermodynamics and equilibrium phase behaviour of charged colloidal suspensions have been investigated experimentally [1–6] and numerically [5–8]. When the concentration of added ions is high, which strongly screens the electrostatic repulsions between the particles, increasing ϕ results in a fluid–fcc solid transition. At low ionic strengths, a fluid–bcc solid transition is observed upon increasing ϕ. Increasing ϕ further in the latter case causes a structural transition from bcc to fcc of the solid in equilibrium with the fluid. A triple point occurs where the fluid, fcc solid and the bcc solid coexist. Recent simulations of the Yukawa system suggest that the fluid–fcc solid transition becomes preferred again at very low ionic strengths, and multiple triple points are identified [8]. However, this re-entrant fcc–bcc–fcc transition has not been observed experimentally.

Currently, no satisfactory descriptions of the solid–solid transition in charged colloidal suspensions exist. To understand the fluid–solid phase transition, Russel *et al* [1] developed a perturbation theory approach to determine the effective hard-sphere size of the charged particles in suspension. Solution properties are then determined as the properties of the effective hard-sphere suspension. Russel *et al* found that this approach captured the phase behaviour reported by Hachisu *et al* [3] quite accurately. However, the approach fails to capture the observations of Monovoukas and Gast [2], who found their data to be in excellent agreement with the simulations of Robbins *et al* [7]. The latter simulations assumed point particles (no hard core)

and are therefore accurate representations of charged particles at low volume fractions and long-range repulsions (low screening). The perturbation theory of Russel *et al* [1], on the other hand, works best for moderate volume fraction samples with highly screened repulsions, where the particles are expected to behave like effective hard spheres. In the limit of low screening, the tail of the perturbation becomes important, and for very high volume fractions, the theory predicts an unphysical overlap of the effective hard spheres.

In an attempt to reconcile these differences, Voegtli and Zukoski [5] developed a perturbation approach, where, following Kang *et al* [21], the effective hard-sphere diameter is determined in a way that prevents the overlap of effective hard spheres until the true hard cores of the particles are close packed. The solution properties are then determined by accounting for the contributions of both the effective hard-sphere and the repulsive tail of the interactions. The resulting predictions capture their own data [5, 6] and the data of Hachisu *et al* [3], Monovoukas and Gast [2], and the simulation data of Robbins *et al* [7]. However, the theory is based on a description of pair interactions alone and as such does not account explicitly for electroneutrality [6]. It is therefore accurate for cases where the ionic strength is well determined by the background salt and the screening from counter ions balancing the charge on the particles is negligible.

Here, we follow Voegtli and Zukoski [5] and Kang *et al* [21] to determine how the effective hard-sphere size will vary with volume fraction. The theory of Kang *et al* is especially useful in the dense limit as in the case of crystallization. According to Kang *et al*, the effective hard-sphere radius, a_{eff}, of the charged particles interacting with the Yukawa potential is given by:

$$a_{eff} = a_{BH}\left(1 + \frac{\sigma_1 \delta}{2\sigma_o}\right) \tag{2}$$

where

$$a_{BH} = \frac{1}{2}\int_0^{\lambda} \mathrm{d}r\left(1 - \exp\left(-\frac{V_o(r)}{kT}\right)\right) \tag{3}$$

and

$$V_o(r) = V(r) - V(\lambda) + (\lambda - r)\left[\frac{\mathrm{d}V(r)}{\mathrm{d}r}\right]_{r=\lambda}. \tag{4}$$

Here, $V(r)$ is given by equation (1) and

$$\frac{\lambda}{2a} = 2^{1/6}\left(\frac{\pi}{6\phi}\right)^{1/3}. \tag{5}$$

The remaining terms in equation (2) are determined as:

$$\delta = \int_0^{\lambda} \mathrm{d}r\left(\frac{r}{2a_{BH}} - 1\right)^2 \frac{\mathrm{d}}{\mathrm{d}r}\left[\exp\left(-\frac{V_o(r)}{kT}\right)\right] \tag{6}$$

$$\sigma_o = \frac{1 - \phi_{eff}/2}{(1 - \phi_{eff})^3} \tag{7}$$

and

$$\sigma_1 = \frac{2 - 7.5\phi_{eff} + 0.5\phi_{eff}^2 - 5.7865\phi_{eff}^3 - 1.51\phi_{eff}^4}{(1 - \phi_{eff})^4} \tag{8}$$

where ϕ_{eff} is the effective hard-sphere volume fraction of the particles given by

$$\phi_{eff} = \sigma^3 \phi \tag{9}$$

with $\sigma = a_{eff}/a$. Solving the above set of equations, the effective hard-sphere radius, a_{eff}, and therefore the ratio σ, can be determined as a function of ϕ, a, and the interaction parameters ε and κ. The model developed by Voegtli and Zukoski [5] then allows the determination of the thermodynamic properties and the resulting phase behaviour of the suspension. However, this requires intensive numerical effort. In the limit of high screening and low charge, Voegtli and Zukoski [5, 6] found that, as suggested by Russel *et al* [1], the phase behaviour is well approximated by mapping onto the effective hard-sphere suspension and neglecting the repulsive tail. Here, we choose the effective hard-sphere description to determine the thermodynamic properties of charged systems. This requires little numerical effort compared to the full-blown perturbation theory calculations, and yet allows us to explore the effects of the strength and range of particle repulsions on the kinetics of crystal nucleation in charged colloidal suspensions, which forms the aim of this paper.

In the effective hard-sphere description, the osmotic pressure, P_f, of the suspension is well approximated by the Carnahan–Starling equation [22]:

$$\frac{4\pi a_{eff}^3 P_f}{3\phi_{eff} kT} = \frac{1 + \phi_{eff} + \phi_{eff}^2 - \phi_{eff}^3}{(1 - \phi_{eff})^3}. \tag{10}$$

The solid phase follows the equation of state [23]:

$$\frac{4\pi a_{eff}^3 P_s}{3\phi_{xeff} kT} = \frac{2.17}{0.738 - \phi_{xeff}} \tag{11}$$

where ϕ_{xeff} is the effective packing fraction in the solid phase. From the osmotic pressure, the chemical potential of a particle in either phase can be determined as [12]:

$$\frac{\mu}{kT} = \int \left(\frac{4\pi a_{eff}^3 P}{3\phi_{eff} kT} - 1 \right) \frac{\mathrm{d}\phi_{eff}}{\phi_{eff}} + \frac{4\pi a_{eff}^3 P}{3\phi_{eff} kT} + C \tag{12}$$

where C is an arbitrary constant. Equating the pressures and the chemical potentials of the solid and the fluid phases provides the effective volume fractions of the coexisting solid and fluid phases at equilibrium. These volume fractions are 0.55 and 0.495, respectively. The fluid phase volume fraction at this equilibrium sets the solubility boundary, $\phi_s = 0.495/\sigma^3$, marking the onset of crystallization. Increasing fractions of the suspension are crystallized as ϕ is increased above ϕ_s until at $\phi_m = 0.55/\sigma^3$ all of the suspension is crystallized.

Two approaches are taken to test the limits of the assumptions made here. First, we compare predictions of the phase transition boundaries with experimental results. Second, we compare our predictions with those of more detailed numerical simulations. We present in figure 1(a) comparisons with the data of Monovoukas and Gast [2] of the location of the fluid–solid boundary as a function of ionic strength. Monovoukas and Gast determine the dimensionless surface potential and charge on their particles to be $\Psi = 2.49$ and $Q = 12.82$, respectively. With these values, the interaction parameters in equation (1) are determined as $\varepsilon/kT = 0.5(a/l)\Psi^2$ and $\kappa = 2[(2N - 3Q\phi)/(1 - \phi)]^{1/2}$, where $N = 4\pi a^2 l N_A[I] \times 10^3$ is the dimensionless ionic concentration, dependent on the molar ionic strength $[I]$, Avogadro's number, N_A, the particle radius, $a = 66.7$ nm, and $l = 7.13 \times 10^{-10}$ m is the Bjerrum length. We note that by calculating κ as a function of ϕ, the model improves on the perturbation theory of Voegtli and Zukoski by accounting for screening by counter ions. Mapping onto the effective hard-sphere description to determine ϕ_s and ϕ_m captures the experimental phase diagram quite well. The agreement is particularly good at high ionic strengths, where the effective hard-sphere description is expected to work best. At low ionic strengths, the model underpredicts the volume fraction at the solubility boundary. Under these conditions, where the screening length is large (see inset), the tail of the repulsive interactions contributes significantly to

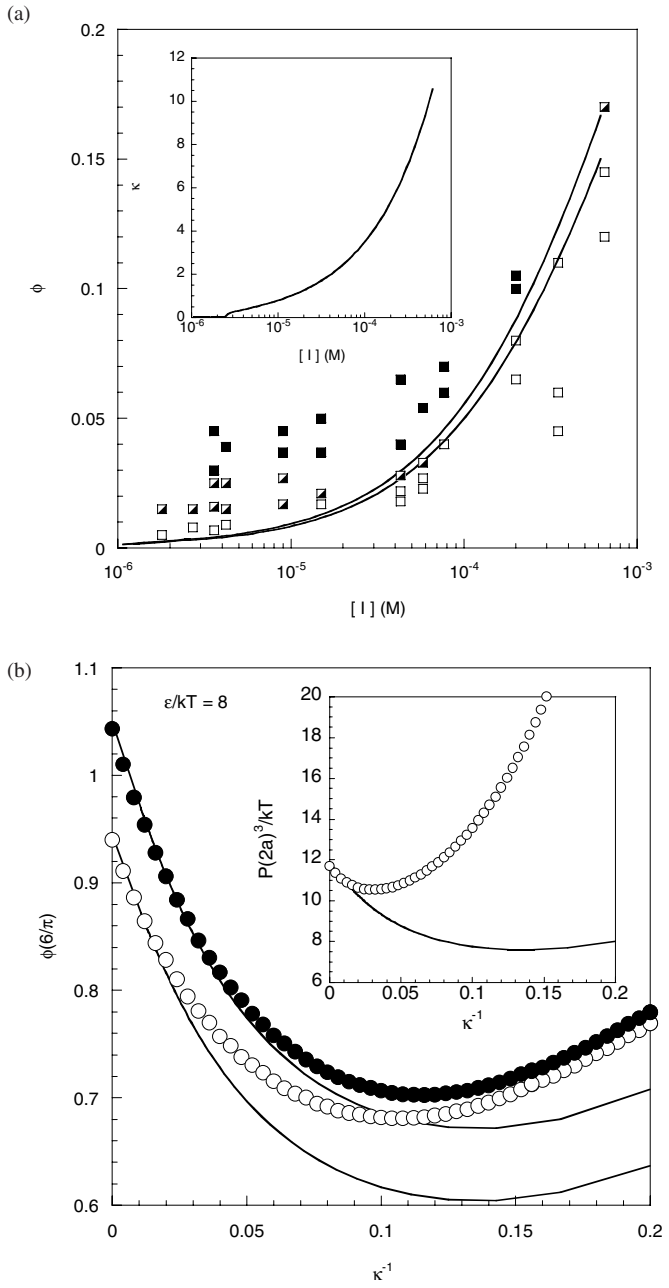

Figure 1. (a) Fluid–crystal coexistence curves (solid curves) calculated using the effective hard-sphere model, as described in the text, compared with the experimental data (symbols) of Monovoukas and Gast [2] as a function of ionic strength of KCl. The lower curve corresponds to $\phi_{seff} = 0.495$ and the upper curve, $\phi_{meff} = 0.55$. The open symbols represent fluid conditions, semi-filled symbols, fluid–crystal coexistence, and filled symbols, completely crystalline conditions. The inset shows the inverse Debye screening length at the different ionic strengths. (b) Fluid–crystal coexistence curves (solid curves) calculated using the effective hard-sphere model, as described in the text, for $\varepsilon = 8$ and different values of κ, compared with the simulation data (symbols) of El Azhar *et al* [8]. The lower curve corresponds to $\phi_{seff} = 0.495$ and the upper curve, $\phi_{meff} = 0.55$. The inset shows the osmotic pressure calculated using equation (10) at $\phi_{eff} = 0.495$ compared with the data of El Azhar *et al* [8].

the resulting phase behaviour. The perturbation theory calculations of Voegtli and Zukoski capture the phase behaviour at low ionic strengths much more accurately by accounting for the effects of the repulsive tail. Even their calculations, however, drastically underpredict the width ($\phi_m - \phi_s$) of the coexistence region.

We present in figure 1(b) comparisons of ϕ_s and ϕ_m for $\varepsilon/kT = 8$ and a range of values of κ with the recent simulation results of El Azhar *et al* [8]. Here, κ is assumed to be independent of ϕ. We find yet again that the simple hard-sphere description captures the simulation data quite well. As κ decreases below infinity, ϕ_s and ϕ_m decrease below their hard-sphere values. Decreasing κ further, ϕ_s and ϕ_m reach minima, and for low values of κ, ϕ_s and ϕ_m increase upon decreasing κ. The model captures these qualitative trends observed in the simulations. Quantitatively, the model also captures the simulation data accurately for high κ (>20 for $\varepsilon = 8$), but fails dramatically for low κ. Also shown in figure 1 is the osmotic pressure of the suspension at the solubility boundary determined via simulations for $\varepsilon = 8$ and the same range of values of κ. In this case, the effective hard-sphere description works well for very high κ, failing below $\kappa \sim 50$. We therefore expect the effective hard-sphere description to work in the limit of high κ. Below, we use the effective hard-sphere description assuming κ and ε to be determined independent of ϕ in order to understand the kinetics of crystal nucleation in charged colloidal suspensions.

3. Crystal nucleation kinetics

In a suspension with $\phi > \phi_s$, crystalline clusters nucleate and grow as the result of a competition between two processes, the aggregation of single particles onto and the dissociation of single particles from cluster surfaces. Previously, we have developed descriptions of these processes for hard-sphere suspensions [12, 13]. Here, we extend the descriptions to charged systems.

3.1. Aggregation rate

We consider a crystalline cluster of radius R in a suspension with background particle volume fraction ϕ. Single particles arrive from the bulk suspension onto the surface of the cluster at a rate $\beta = \beta(R, \phi)$. To determine β, we note that when particles compact to form clusters, a zone is created around every cluster that is depleted of particles. That this description applies to charged systems is indicated by the direct observations of Gasser *et al* [20], who found the packing fraction in crystalline clusters to be higher than in the surrounding bulk suspension. The particle volume fraction at large distances from the cluster surface equals the bulk volume fraction, ϕ. A volume fraction gradient is thus established from the surface of the cluster to the bulk suspension. Particles diffuse down this gradient at a rate that is determined by solving the diffusion equation. The result is [12, 13]:

$$\beta_{=} \frac{3R}{a^3}\left(1 + \frac{a_{eff}}{R}\right)\int_{\phi_R}^{\phi} D(\phi')\,\mathrm{d}\phi' \tag{13}$$

where ϕ_R, discussed below, is the packing fraction of particles on the cluster surface, and $D(\phi)$ is the gradient diffusivity of the particles given by:

$$D(\phi) = D_o K_D(\phi) T_D(\phi_{eff}) \tag{14}$$

where $D_o = kT/6\pi\eta a$ is the Stokes–Einstein diffusivity, with η the solvent viscosity. Recognizing that the effective hard-sphere description captures the thermodynamics of charged colloidal suspensions, the thermodynamic contribution to the diffusivity, T_D, is evaluated at

ϕ_{eff} and is given by [1, 12, 13]:

$$T_D(\phi_{eff}) = \frac{\mathrm{d}}{\mathrm{d}\phi_{eff}}[\phi_{eff} Z(\phi_{eff})] \tag{15}$$

where $Z(\phi_{eff}) = 4\pi a_{eff}^3 P_f/\phi_{eff} kT$ and is calculated using equation (10).

The key difference between the description developed here and that developed for hard spheres lies in the description of hydrodynamic interactions. The no slip boundary condition characterizing the hydrodynamic drag occurs at the core particle surface and therefore depends on ϕ as opposed to ϕ_{eff} and is approximated as [1, 12, 13]:

$$K_D(\phi) = (1-\phi)^{-K_2} \tag{16}$$

where the exponent K_2 is a function of the interactions between the particles. Russel *et al* [1] developed approximations for K_2 for charged suspensions by assuming that the particles interact via an excluded shell potential. Here, following Russel *et al*, we write:

$$K_2 = -6\sigma^2 + 1 - \frac{15}{8\sigma} + \frac{9}{64\sigma^3} + \frac{107}{640\sigma^5} + \Theta(\sigma^{-7}) \tag{17}$$

where $\sigma = a_{eff}/a$. Note that $K_2 = -6.567$ when $\sigma = 1$, yielding the hard-sphere limit. For charged sphere suspensions, this description has been tested in the dilute limit by measuring the particle diffusivity using scattering techniques [1, 24]. Here, we assume this description to also hold for dense suspensions. Combining equations (13)–(17) yields the aggregation rate, β, of particles onto a cluster surface.

3.2. Dissociation rate

To determine the dissociation rate, particles on a cluster surface are assumed to reside in potential energy wells because of their bonds with their nearest neighbours. As in hard-sphere suspensions, the strength of interparticle bonds on a cluster surface is determined by the potential of mean force [12, 13]. The latter potential is calculated using the effective packing fraction of particles on the cluster surface, $\phi_{Reff} = \sigma^3\phi_R$, where ϕ_R is given by equation (20) below. The motion of surface particles in their potential wells is described by the Smoluchowski equation. Solving the Smoluchowski equation using the mean first passage time analysis, the rate α at which particles dissociate from the cluster surface is determined to be [12, 13]:

$$\alpha = \frac{6\omega D_o \phi_{Reff} R}{a_{eff}^3} \frac{[1-(1-a_{eff}/R)^3]}{[1-a_{eff}/2R]} \frac{[1+a_{eff}/R]^2}{[(1+a_{eff}/R)^3-1]} \left[\frac{(1-\phi_{Reff})^3}{(1-\phi_{Reff}/2)}\right]^{C_s-C_f} \tag{18}$$

where D_o is the Stokes–Einstein diffusivity of the particles, and ω is an approximate correction to D_o due to the near field hydrodynamic interactions between the particles on the cluster surface. For the hard-sphere case, nearest neighbours are assumed to be nearly touching so that $\omega = 0.2$ provides a good estimate of the hydrodynamic correction [12, 13]. For charged systems, although the particle centres are arranged in a manner identical to that of hard spheres, the particle surfaces are sufficiently separated (unless $\sigma \sim 1$) that near field hydrodynamic interactions can be neglected. Here, we let $\omega = 1.0$ for all our calculations.

The number of bonds, C_s, of a particle on the cluster surface depends on the cluster radius, R, as [12, 13]:

$$C_s - C_f = (C_{s\infty} - C_f)(1 - \exp\{\zeta(R_{min} - R)/2a_{eff}\}) \tag{19}$$

and determines the depth of the potential well in which the surface particles reside. Here, $C_{s\infty}$ is the number of nearest neighbours of a particle on the surface of an infinitely large cluster and

C_f is the number of nearest neighbours of a particle in the fluid. $R_{min} = a_{eff}(2/0.74)^{1/3}$ is the radius of the smallest possible cluster, i.e., containing two particles. The above form for $C_s(R)$ is an empirical interpolation, where the parameter ζ controls the rate of increase of C_s from C_f to $C_{s\infty}$ as R increases. This parameter can, in principle, be determined independently. In addition, ζ is related to the curvature dependence of the solid–fluid surface tension [12, 13]. However, this latter dependence for charged colloidal systems is not known. For hard-sphere systems, $\zeta = 0.9$ results in a good comparison of experimental estimates and model predictions of several measures of crystal nucleation kinetics [13]. Here, we assume this value to hold for charged systems as well. Similarly, for hard-sphere suspensions, $C_{s\infty}$ is determined from knowledge of the interfacial tension of an infinitely large crystalline surface in equilibrium with the bulk suspension at the solubility boundary. Again, since such information for charged systems is not available, we proceed with the hard-sphere value, $C_{s\infty} - C_f = 2.0$, for the present calculations [13]. We note that use of the hard-sphere values for the parameters ζ and $C_{s\infty} - C_f$ is an approximation, but is reasonable since we expect the effective hard-sphere description to successfully describe particle packing profiles on cluster surfaces in charged systems.

Extending the hard-sphere description, we let the packing fraction of particles on a cluster surface, ϕ_R, depend on ϕ as [12, 13]:

$$\phi_{Reff} = \phi_{RSeff} + (0.64 - \phi_{RSeff}) \exp\{\xi(\phi_{eff} - 0.64)/(\phi_{eff} - 0.495)\} \quad (20)$$

where $\phi_{Reff} = \phi_R\sigma^3$, and ϕ_{RSeff} is the value of ϕ_{Reff} when $\phi = \phi_s$ (or when $\phi_{eff} = 0.495$). Again, the form for ϕ_R is an empirical interpolation where the parameter ξ characterizes how the density of particles in the surface layer changes with the suspension volume fraction. This parameter is related to the volume fraction dependence of the solid–fluid surface tension, and drawing from the hard-sphere value [13] for lack of further information we set $\xi = 1.0$ for the present calculations.

To determine ϕ_{RSeff}, we note that only infinitely large clusters are stable at the solubility boundary. The stability of clusters is determined by the relative values of the aggregation and dissociation rates, β and α, respectively. In general, when $\phi > \phi_s$, $\beta < \alpha$ for small clusters and vice versa for large clusters. The critical cluster size, R^*, is defined as that size at any ϕ at which $\beta = \alpha$. Clusters smaller than the critical size tend to shrink, whereas larger clusters tend to grow. At the solubility boundary, R^* diverges. Thus, writing $\beta = \alpha$ as $R \to \infty$ for $\phi = \phi_s$ yields:

$$\int_{\phi_{RS}}^{\phi_s} \frac{D(\phi')}{D_o}\,\mathrm{d}\phi' = 2\omega\phi_{RS}\left[\frac{(1-\phi_{RSeff})^3}{1-\phi_{RSeff}/2}\right]^{C_{s\infty}-C_f} \quad (21)$$

where $\phi_{RS} = \phi_{RSeff}/\sigma^3$, and $D(\phi)$ is given by equations (14)–(17). Solving this equation determines ϕ_{RS}, thereby allowing the calculation of both the aggregation and dissociation rates as functions of R, ϕ, ε and κ.

3.3. Pseudo-steady nucleation rate

As ϕ increases above ϕ_s, the critical cluster size, R^*, decreases to finite values of R and stable crystalline clusters form. At any $\phi/\phi_s > 1$, the rate at which clusters of the critical size form is taken as the nucleation rate. As crystallization progresses, a distribution of cluster sizes is established in the suspension. Detailed population balance models, allowing for the evolution of the cluster size distribution (and drop in monomer concentration as more and larger clusters are formed), demonstrate that, after a transient period, the nucleation rate attains a steady value [13]. Standard approaches based on free energies of cluster formation assume that the

background monomer volume fraction, ϕ, stays constant as crystals nucleate [25]. However, population balance equations that conserve the mass of particles in the suspension indicate that as crystallization progresses, ϕ (the concentration of monomers not in clusters) quickly reduces to a lower value ϕ_{plat} and remains constant at this value for a significant period of time [13]. Calculations of steady state nucleation rates assuming that ϕ is reduced to ϕ_{plat} result in much better comparisons with experiments than calculations that assume ϕ to remain constant [13]. Thus without solving detailed population balance equations, a good estimate of the nucleation rate at ϕ can be obtained by calculating the nucleation rate at $\phi_{plat}(\phi)$. At any value of ϕ, ϕ_{plat} is estimated by assuming that all of the particles are either monomers or dimers. A steady distribution of monomers and dimers is then postulated and the concentration of monomers, ϕ_{plat}, is found by assuming that equilibrium is established. The resulting balance yields [13]:

$$\phi_{plat} = \frac{\phi}{1 + \frac{2\beta(1,\phi_{plat})}{\alpha(2,\phi_{plat})}\left[1 - \frac{\phi}{\phi_x(\phi_{plat})}\right]} \tag{22}$$

where $\beta(1, \phi_{plat})$ and $\alpha(2, \phi_{plat})$ are the rates of the aggregation of pairs of monomers and the dissociation of dimers, respectively. As the population of trimers and higher aggregates is smaller than monomers and dimers for much of the nucleation process, equation (14) is found to provide an excellent estimate of the pseudo-steady-state monomer concentration [13]. Further, $\phi_x = \phi_{xeff}/\sigma^3$, where ϕ_{xeff}, the effective packing fraction in the solid phase, is obtained by assuming all clusters to be in mechanical equilibrium with the surrounding fluid [12, 13]. From the known equations of state for the solid and fluid phases, this yields:

$$\phi_{xeff} = \frac{0.738}{1 + \frac{2.17(1-\phi_{eff})^3}{(1+\phi_{eff}+\phi_{eff}^2-\phi_{eff}^3)\phi_{eff}}}. \tag{23}$$

At any ϕ, the steady state nucleation rate is then estimated by the equation [12]:

$$J(\phi) = \frac{3\beta\phi_{plat}}{8\pi a^3}\left(\frac{w''(g^*)}{\pi}\right)^{1/2} \exp(2w(g^*)) \tag{24}$$

where

$$w(g) = \int_0^g \frac{\beta - \alpha}{\beta + \alpha}\,\mathrm{d}g. \tag{25}$$

with $g = \phi_{xeff}(R/a_{eff})^3$ and $g^* = \phi_{xeff}(R^*/a_{eff})^3$. Here, α, β, and R^* are calculated at $\phi_{plat}(\phi)$.

4. Model calculations

We present in figure 2 calculations using equation (24) of the pseudo-steady-state nucleation rate, J, as a function of the effective hard-sphere volume fraction, ϕ_{eff}, for different values of ε at a fixed value of $\kappa = 10$. For $\phi_{eff} > 0.495$, the size ratio, σ, the effective plateau volume fraction, ϕ_{plat}, and the critical cluster size, R^*, are plotted as functions of ϕ_{eff} in figures 3–5, respectively, for all the cases considered in figure 2. Where relevant, the corresponding quantities for the hard-sphere case are also presented for comparison. The inset in figure 4 shows how ϕ_s changes with ε for $\kappa = 10$.

Interestingly, we find that nucleation rates vary non-monotonically upon increasing ε at a fixed κ: as shown in figure 2, at a fixed ϕ_{eff}, J first decreases below the hard-sphere value and then increases upon increasing ε. For large increases in ε, J appears to saturate, as in figure 2 for $\varepsilon/kT = 60$. The location of the maximum in the nucleation rate, which occurs at $\phi \sim 0.55$ for hard-spheres, gradually shifts to higher values of ϕ_{eff} as ε increases. Below,

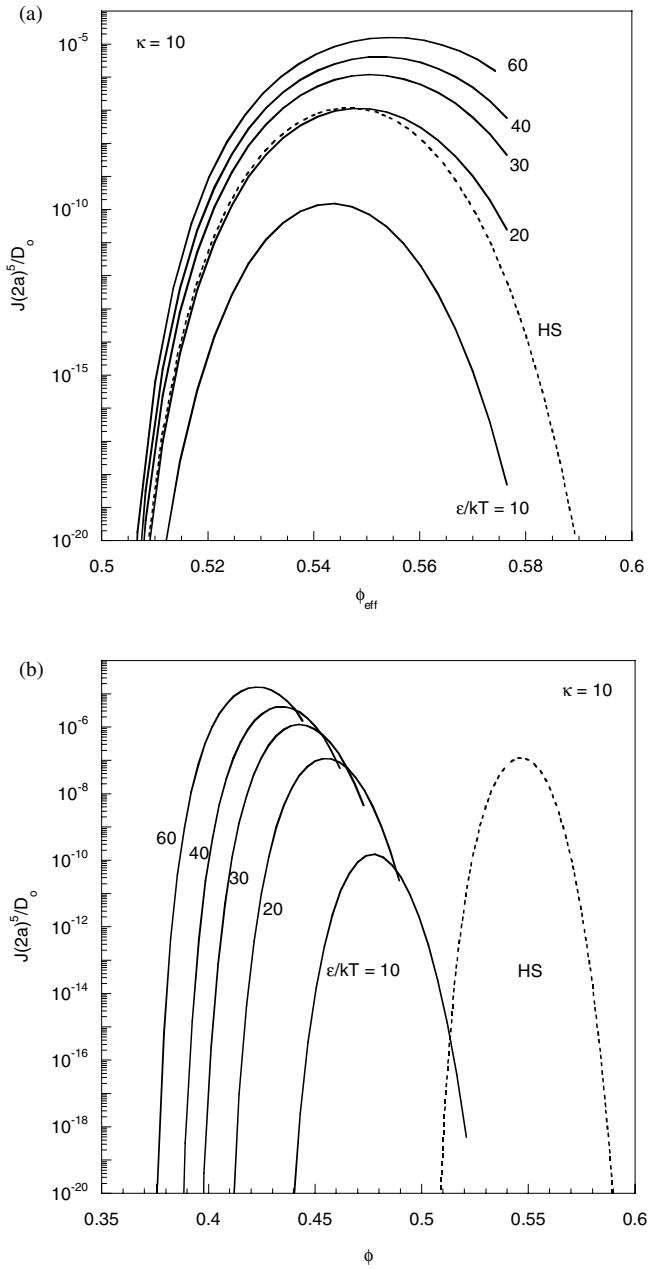

Figure 2. Nucleation rates calculated using equation (24) as functions of (a) the effective hard-sphere volume fraction and (b) the actual particle volume fractions for $\kappa = 10$ and different values of ε.

we explain these observations based on our description of the underlying particle aggregation and dissociation processes for purely repulsive systems.

The decrease in J below the hard-sphere value is attributed to the near field hydrodynamic interactions between the particles on cluster surfaces. These interactions determine the

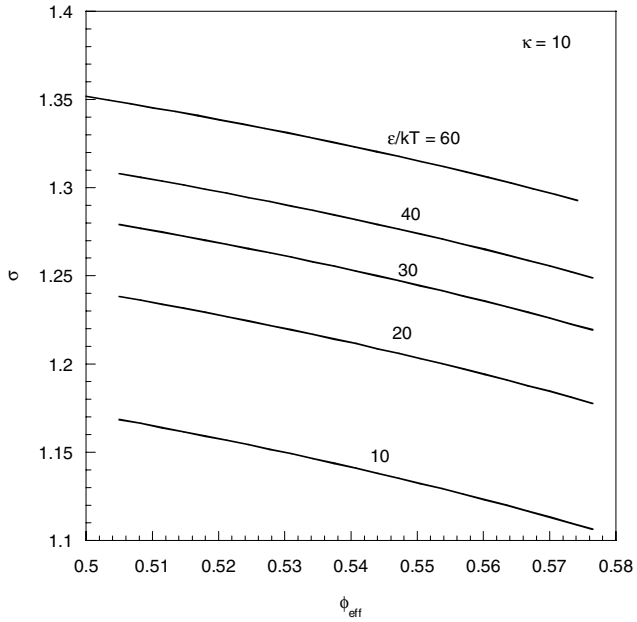

Figure 3. Ratio of the effective hard-sphere size to the particle size calculated using equations (1)–(9) for $\kappa = 10$ and different values of ε.

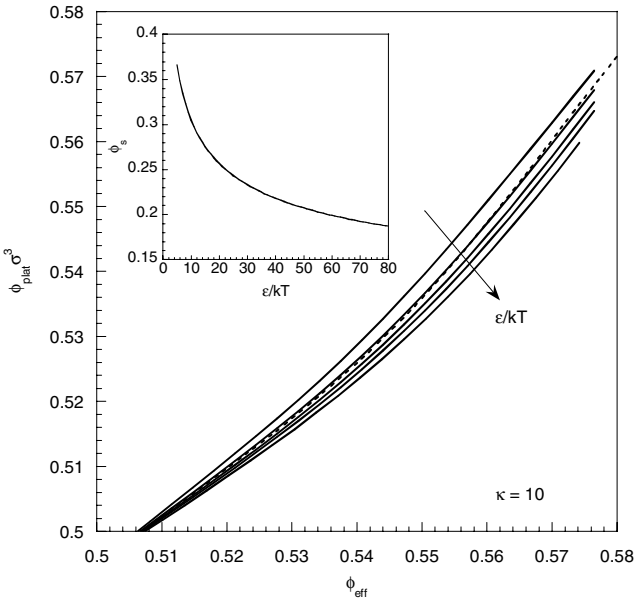

Figure 4. Plateau volume fractions calculated using equation (22) for $\kappa = 10$ and different values of ε. The inset shows the variation of ϕ_s under the same conditions.

diffusivity of particles in the potential wells holding them on cluster surfaces and therefore affect the rate of particle dissociation, α, given by equation (18) above. For hard spheres, the hydrodynamic interactions are assumed to reduce the particle diffusivity on the cluster surface

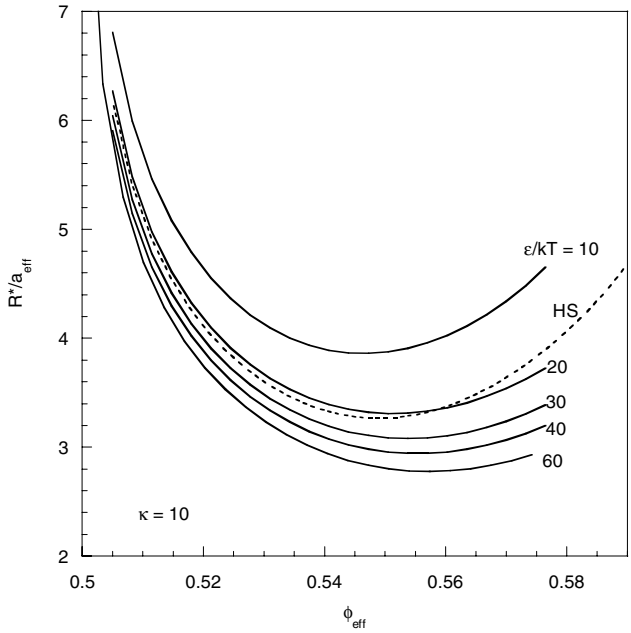

Figure 5. Critical cluster radii calculated by equating the aggregation and dissociation rates given by equations (13) and (18), respectively, for $\kappa = 10$ and different values of ε.

to 20% of the Stokes–Einstein diffusivity, as indicated by the value of 0.2 chosen for ω in equation (18). For charged spheres interacting with the excluded shell potential, near field hydrodynamic interactions are assumed to be absent and ω is set to 1. At a fixed value of ϕ_{eff}, the dissociation rate α is therefore higher for charged systems than for hard spheres. This makes crystal nucleation difficult and J decreases as ε/kT increases from 0 to 10 at a fixed κ in figure 2.

Increasing ε/kT beyond 10 (in figure 2), near field hydrodynamic effects play no role as ω remains fixed at 1. However, an increase in $\sigma = a_{eff}/a$, as shown in figure 3, results. At any ϕ_{eff}, as indicated in equation (15), the thermodynamic contribution to the particle diffusivity is independent of σ. Combining equations (16) and (17), the hydrodynamic contribution may be written up to the leading order term in $1/\sigma$ as $K_D(\phi) = 1 - 6\phi_{eff}/\sigma$. Thus, at a fixed ϕ_{eff}, $K_D(\phi)$ increases upon increasing σ. In other words, particles diffuse faster as their true size gets smaller at a fixed effective hard-sphere size. The result is that at any ϕ_{eff}, the particle aggregation rate, β, increases upon increasing ε at a fixed κ. This increase in β causes J to increase as ε increases (beyond 10 in figure 2) for fixed κ.

The above effects also explain the gradual shift of the location of the maximum in J to higher ϕ_{eff} upon increasing ε in figure 2. For hard-sphere suspensions, the maximum occurs at $\phi \sim 0.55$. As discussed before, this is the result of a competition between thermodynamic and particle crowding effects: J increases upon increasing ϕ above ϕ_s due to an increasing thermodynamic driving force. Approaching $\phi = 0.64$, however, where particles are randomly close packed, the gradient in the concentration of particles from the bulk suspension to cluster surfaces vanishes. The aggregation rate of particles is therefore greatly diminished and J drops. The result is a maximum in J at $\phi \sim 0.55$. For charged suspensions, the same competition exists except that dependencies of α and β on ϕ_{eff} are altered due to changes in σ. Increasing ε at fixed κ results in an increase in $K_D(\phi)$ as discussed above. In order for β to remain constant,

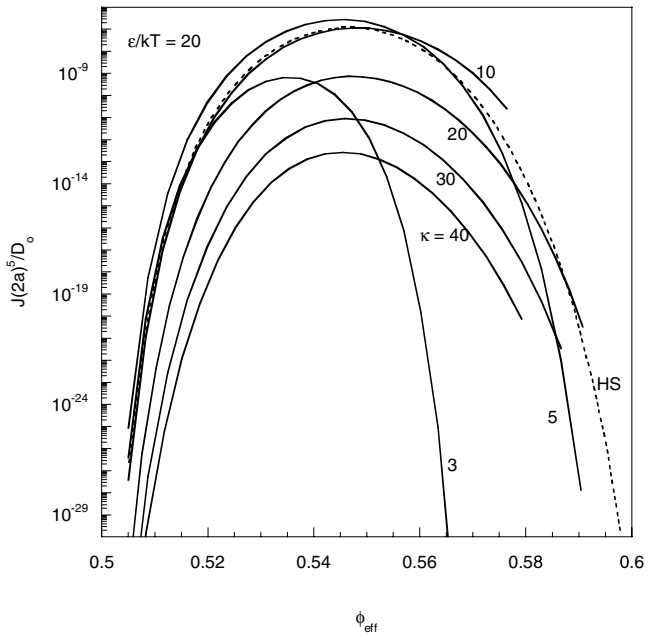

Figure 6. Nucleation rates calculated using equation (24) as functions of the effective hard-sphere volume fraction for $\varepsilon/kT = 20$ and different values of κ.

the increase in $K_D(\phi)$ must be compensated by a lower concentration gradient, which requires a higher ϕ_{eff}, i.e., ϕ_{eff} closer to 0.64. The maximum in the nucleation rate is therefore shifted to higher values of ϕ_{eff} as σ increases, which in figure 2 is produced by increasing ε.

We note that the reduction in J upon increasing ε from 0 to 10 is the result of approximating particle interactions using an excluded shell potential. In general, one expects the near field hydrodynamic interactions to be reduced gradually upon increasing σ until they vanish for $\sigma \gg 1$. The excluded shell model is rigorously applicable only for $\sigma \gg 1$. Its use in our calculations, where $\sigma \sim 1$, introduces uncertainties in the quantitative estimates of J. The qualitative trends predicted, however, are based on reasonable descriptions of the particle aggregation and dissociation processes and are expected to hold.

Next we present in figure 6 calculations of J using equation (24) for different values of κ at a fixed value of $\varepsilon = 20$. We find J to vary much more sensitively with κ than ε. Again, J first decreases below the hard-sphere value upon decreasing κ (hard spheres correspond to $\kappa = \infty$) due to the absence of near field hydrodynamic interactions. Decreasing κ further causes an increase in J up to $\kappa = 10$. This is due to an increase in σ which causes an increase in β as described above. The location of the maximum in J also shifts to higher ϕ_{eff}. Decreasing κ below 10, however, causes a reversal of these trends. J begins to decrease and the location of the maximum shifts to lower ϕ_{eff}.

To understand this reversal, we present in figure 7 calculations of σ_s, the value of σ at the solubility boundary $\phi_{eff} = 0.495$, for different values of ε and κ. Here, σ_s is determined by solving equations (1)–(9). As expected, at any κ, σ_s increases with ε, and at any ε, σ_s increases upon decreasing κ. However, decreasing κ below a certain ε dependent value, which we denote κ_{min}, produces a reversal in the trend and σ_s begins to decrease. (At any ε, κ_{min} may be defined as that value of κ at which σ_s attains its maximum for that ε.) Thus, at a fixed ε, decreasing κ causes ϕ_s to decrease first ($\kappa > \kappa_{min}$) and subsequently increase ($\kappa < \kappa_{min}$)

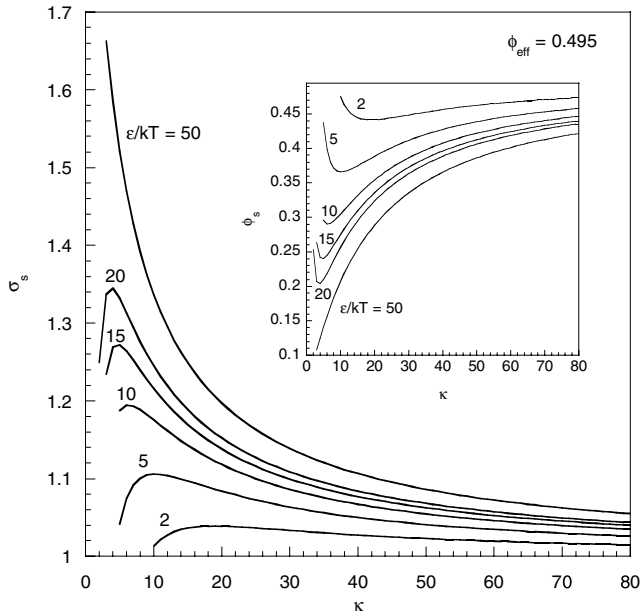

Figure 7. Ratio of the effective hard-sphere size to the particle size calculated using equations (1)–(9) at the solubility boundary as a function of κ=10 for different values of ε. The inset shows the corresponding volume fractions at the solubility boundary.

(inset in figure 7). This subsequent decrease in σ_s upon decreasing κ below κ_{min} explains the reduction in the nucleation rates, J, observed in figure 6 for $\kappa < 10$. As σ decreases, $K_D(\phi)$ becomes smaller at any ϕ_{eff} and causes β to decrease. The result is a decrease in J upon decreasing κ below 10 in figure 6. Auer and Frenkel [19] also observed nucleation rates to first increase and then decrease upon decreasing κ at a fixed ε. The latter decrease is attributed to the non-monotonic variation of ϕ_s with κ at a fixed ε, which is also observed in simulations of the phase behaviour of Yukawa particles [8] as shown in figure 1.

To understand the shift in the location of the maximum in J under these conditions, we present in figure 8, changes in σ, i.e., the effective hard-sphere size of the particles, with increasing ϕ_{eff} for all the cases considered in figure 6. As expected, σ decreases monotonically upon increasing ϕ_{eff} for all values of κ. At any ϕ_{eff}, σ increases upon decreasing κ up to 10 and then begins to decrease. This is consistent with the observation in figure 7 that ϕ_s first decreases ($\kappa > \kappa_{min}$) and then increases ($\kappa < \kappa_{min}$) upon decreasing κ at a fixed ε. Thus at any ϕ_{eff}, the actual volume fraction ϕ increases as κ decreases below κ_{min}. Correspondingly, $K_D(\phi)$ decreases and particles diffuse more slowly, with the result that maximum in J shifts to lower ϕ_{eff}.

The above discussion of model calculations explains the variation of nucleation rates with the strength and the range of particle repulsions and points to the rich physics underlying the kinetics of crystal nucleation in charged colloidal suspensions. To test this description, we turn next to a comparison of model calculations with experiments and simulations.

5. Comparisons with experiments and simulations

The kinetics of crystallization in hard-sphere suspensions has been well studied [2, 9], but few experiments have been reported on charged colloidal suspensions. Here, we compare

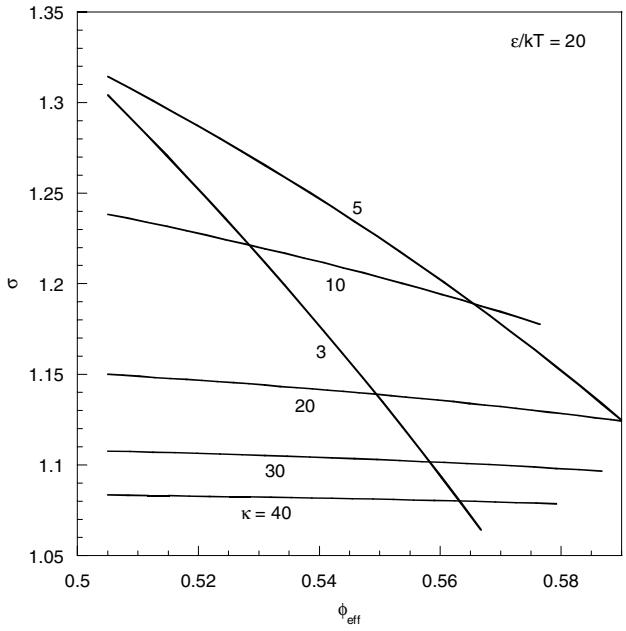

Figure 8. Ratio of the effective hard-sphere size to the particle size calculated using equations (1)–(9) for $\varepsilon/kT = 20$ and different values of κ.

our predictions with the experiments of Dhont *et al* [16], who investigated crystallization kinetics in charged silica suspensions. The phase boundary for their system occurs at $\phi_s \sim 0.194$. They estimate the Debye screening length at the solubility boundary to be 43 nm. Since their particles are ∼160 nm in radius, this yields the Yukawa parameter $\kappa \sim 320/43 = 7.44$. The effective hard-sphere radius at the solubility boundary is given by the ratio $\sigma_s \sim (0.495/0.194)^{1/3} = 1.367$. Thus, to mimic their experimental conditions, we choose the other Yukawa parameter, ε, to yield $\sigma_s \sim 1.367$ for $\kappa = 7.44$. We find that $\sigma_s = 1.37$ for $\varepsilon = 37.0$. We calculate nucleation rates using equation (24) for these values of κ and ε and compare with the experiments of Dhont *et al* in figure 9.

The experimental data presented in figure 9 has been obtained from the nucleation rates reported by Dhont *et al* as follows. Dhont *et al* measure the intensity of light scattered by a crystallizing sample as a function of time. Typically, after an initial transient period, the intensity rises at a fixed, concentration dependent, rate and eventually reaches a plateau. The duration of the transient period is taken as an induction time. From the plateau intensity at long times, the number of crystals, assumed to be of a constant size, in the scattering volume is determined. Assuming that all these crystals nucleate during the transient period, the ratio of the number of crystals and the induction time is reported as the nucleation rate (in units of s^{-1}). To compare with model calculations, we divide the reported rates with the scattering volume (50–300 mm^3) and then non-dimensionalize the rates with $(2a)^5/D_o$, where we use the reported value of $a = 160$ nm and estimate $D_o = 1.5 \times 10^{-8}$ cm^2 s^{-1} for their particles suspended in a mixture of ethanol and toluene.

As shown in figure 9, the model captures the qualitative features of the experimental nucleation rates. The maximum in the nucleation rate observed for hard spheres is no longer seen and both model calculations and experimental estimates of nucleation rates increase monotonically with ϕ. Model calculations do predict the maximum, however, but at a value

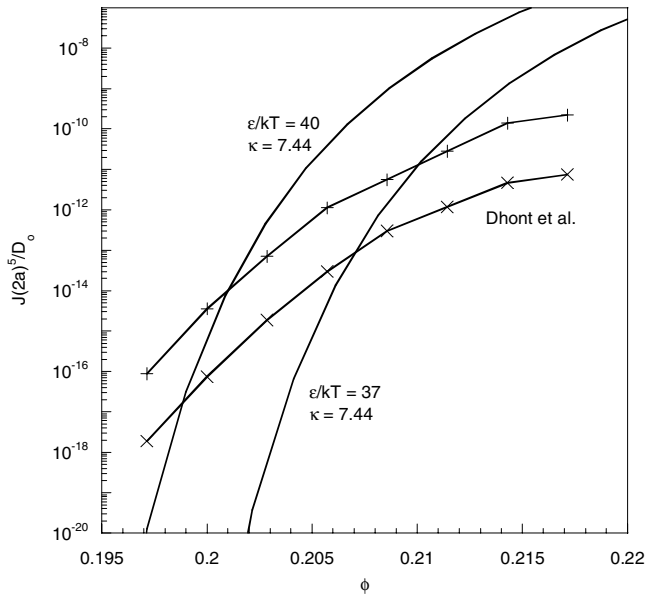

Figure 9. Comparison of nucleation rates calculated (solid curves) using equation (24) for the values of ε and κ shown with the maximum (+) and minimum ($\times$) rates reported by Dhont *et al* [16].

of ϕ outside the range of the experiments. This explains why the maximum in the rates is not observed in some of the experiments on charged systems. Quantitatively, the model predicts a much sharper rise in the nucleation rates with ϕ than is observed in the experiments. For instance, increasing ϕ from 0.2 to 0.215, the model predicts an increase in J of nearly 20 orders of magnitude, whereas experimentally, J is observed to increase by 6–8 orders of magnitude. One reason for this discrepancy might be the uncertainty in our knowledge of ϕ_s. Nucleation rates change very steeply for $\phi \sim \phi_s$, whereas the change is more modest at higher ϕ.

To account for this uncertainty, we present additional calculations using $\varepsilon = 40.0$ and $\kappa = 7.44$, which yield $\sigma_s = 1.38$, lowering the value of ϕ_s from the value at $\sigma_s = 1.37$ by 2%. Model predictions of nucleation rates with these parameter values are in much better agreement with the experiments. Nevertheless, significant quantitative discrepancies exist, with the model generally overpredicting experimental nucleation rates.

The reasons for the quantitative discrepancies between model predictions and experimental estimates of J are several. Light scattering inherently measures the cumulative effect of all the clusters present in the crystallizing sample. Deconvoluting the measured intensities to nucleation rates is ridden with severe uncertainties. Similarly, linking induction times to underlying nucleation events is extremely difficult. We have recently developed a population balance model that establishes precise links between model parameters and experimental measures of nucleation kinetics obtained from light scattering techniques [13]. From these links, it is clear that the nucleation rate reported by Dhont *et al* is a different quantity from the rate calculated by the present model. Besides, limitations in the model, which we discuss below, also contribute to the discrepancies in the above comparison.

We turn next to the data of Gasser *et al* [20], who conducted real space imaging experiments of crystallizing suspensions of slightly charged particles. We present in figure 10 nucleation rates reported by Gasser *et al*, made dimensionless with $(2a)^5/D_o$, where we use the reported value of $a = 1.26$ μm and estimate $D_o = 6.9 \times 10^{-14}$ m^2 s^{-1}. The solubility boundary for

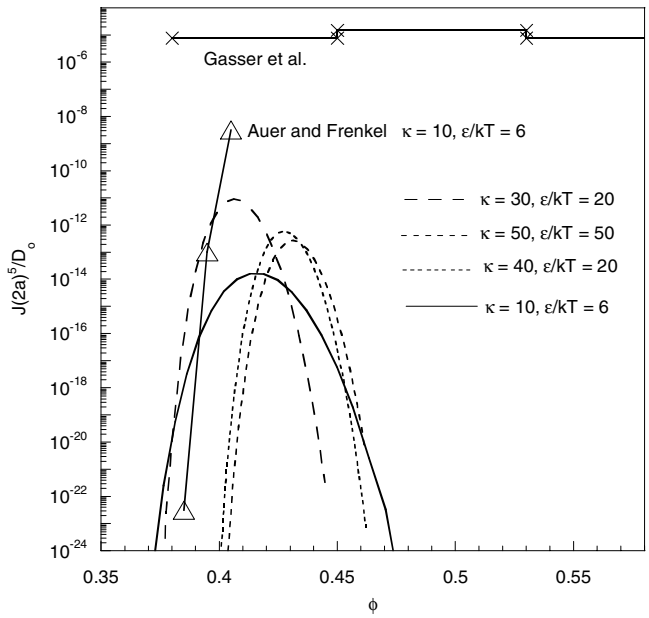

Figure 10. Comparison of nucleation rates calculated using equation (24) for different values of ε and κ shown with the rates reported by Gasser *et al* [20] ($\times$) and Auer and Frenkel [19] (Δ).

their particles is reported to be 0.38, which corresponds to $\sigma_s \sim 1.09$. Several combinations of the Yukawa parameters ε and κ yield this value of σ_s. We present calculations in figure 10 using four combinations of these parameters and compare them with the data of Gasser *et al*. The parameters are chosen such that for any ε, the corresponding value of $\kappa > \kappa_{min}$ (see figure 7). As shown in figure 10, in all cases we find severe discrepancies between model predictions and experimental estimates, the model this time underpredicting nucleation rates by tens of orders of magnitude. As shown in figure 10, Auer and Frenkel [19] also find similar discrepancies between their simulations and the experimental estimates of Gasser *et al*. They attribute the discrepancies to a lack of knowledge of the variation of ε and κ with ϕ.

Finally, we present in figure 11, comparisons of model calculations with the simulation data of Auer and Frenkel [19]. Of the vast amount of data reported by Auer and Frenkel, we choose those combinations of ε and κ for which $\kappa > \kappa_{min}$. Differences between the values of σ_s calculated using the present formulation and those determined by simulations are prominent for $\kappa < \kappa_{min}$ making comparisons of nucleation rates difficult. We compare our calculations of nucleation rates with simulations for the following combinations: $\varepsilon = 8$ and $\kappa = 10$, and $\varepsilon = 20$ and $\kappa = 5$. Even here, we note that we are stretching the limits of the effective hard-sphere description.

In figure 11, nucleation rates, J, are presented as functions of ϕ for each combination of ε and κ. Model calculations compare well with the simulations. The dependence of J on ϕ for small values of ϕ (before the maximum in J) is identical for both the calculations and the simulations. That the curves are laterally shifted (along the ϕ axis) may be attributed to the differences in the estimates of ϕ_s between our calculations and the simulations. For $\varepsilon = 8$ and $\kappa = 10$, $\phi_s = 0.323$ according to our calculations, whereas the simulations yield $\phi_s = 0.354$. Similarly, for $\varepsilon = 20$ and $\kappa = 5$, the two values are 0.210 and 0.262, respectively. To eliminate this uncertainty in ϕ_s in our comparisons of J, we present in figure 12, the data in figure 11 plotted as a function of ϕ/ϕ_s. Here, model calculations agree quantitatively with

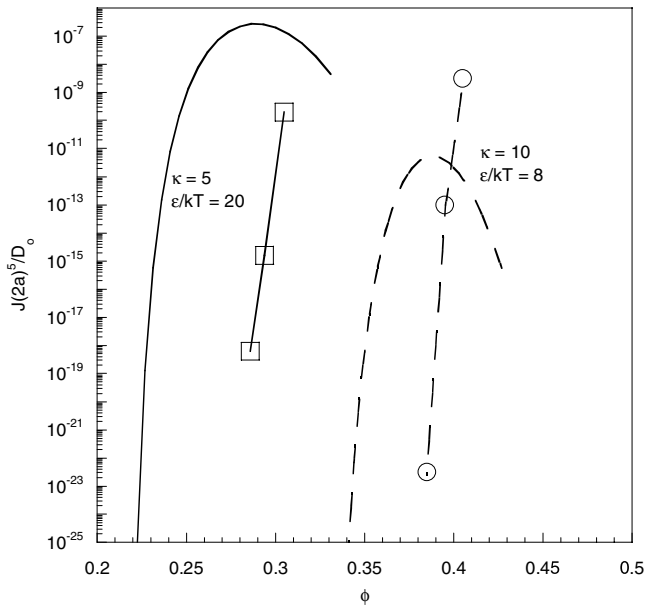

Figure 11. Comparison of nucleation rates calculated using equation (24) with the rates reported by Auer and Frenkel [19] (symbols) for $\varepsilon/kT = 20$ and $\kappa = 5$ (solid curves) and $\varepsilon/kT = 8$ and $\kappa = 10$ (dashed curves).

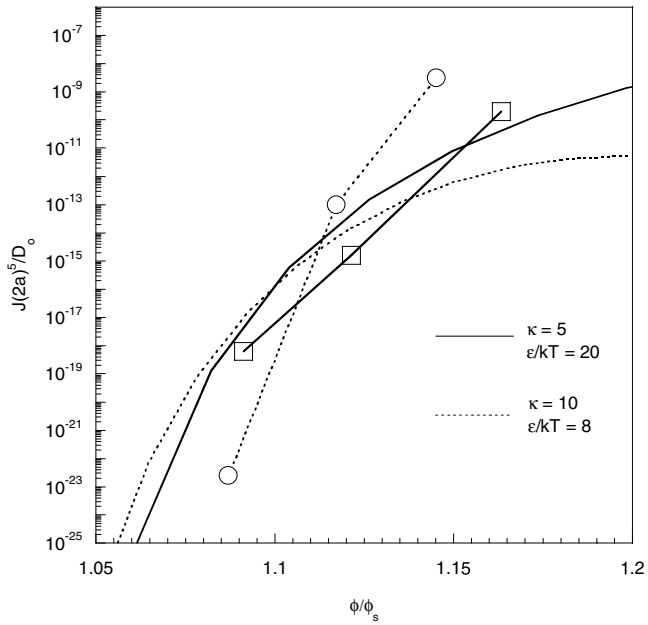

Figure 12. The data of figure 11 plotted as a function of ϕ/ϕ_s.

the simulation data. In particular, we find remarkable agreement for the case of $\varepsilon = 20$ and $\kappa = 5$. For $\varepsilon = 8$ and $\kappa = 10$, however, discrepancies exist between our calculations and simulations. This may be attributed to κ for this case being close to κ_{min} (figure 7). Thus, from the limited comparisons possible, we conclude that for $\kappa \gg \kappa_{min}$, uncertainties exist in

the values of ϕ_s determined, but when compared at constant ϕ/ϕ_s, model calculations of J agree well with simulations. Model predictions are thus in semi-quantitative agreement with the simulations of Auer and Frenkel.

In addition, we note that our model predictions are in excellent qualitative agreement with the simulations of Auer and Frenkel, duplicating the dependencies of J on ε and κ observed in their simulations. At a fixed κ, increasing ε at any ϕ_{eff} results in an increase in J, which asymptotes for large values of ε. Decreasing κ at a fixed ε results first in an increase in J followed by a subsequent decrease. These trends are predicted by the model as shown in figures 2 and 6. However, differences arise between model predictions and simulations on two accounts: first, the simulations do not see the maximum in J predicted by the model. This might be because the simulations are conducted at low values of ϕ so that only the increasing portion of the nucleation rate curves is sampled. The second qualitative difference between model predictions and the simulations is that at any ϕ_{eff}, the nucleation rates estimated by the simulations are consistently higher than the corresponding rates for hard spheres. The model, however, predicts nucleation rates lower than the hard-sphere values due to the effects of near field hydrodynamic interactions. Resolving this latter difference requires more detailed studies where particle interactions are carefully tuned near the hard-sphere limit.

The origin of the quantitative discrepancies between model predictions and simulations may lie in the approximations employed both in the model and in the simulations. Chief among the former is the use of the effective hard-sphere description, which works only for very high κ. For low κ, the description introduces uncertainties in the thermodynamic properties of charged colloidal suspensions. Further, even for the excluded shell model, the description of the gradient diffusivity employed (equations (14)–(17)) has only been tested in the dilute limit. Finally, the use of the hard-sphere values for the parameters $C_{s\infty} - C_f$, ζ and ξ might also introduce uncertainties in model calculations.

Approximations in the simulations include the use of an *ad hoc* scaling for determining the particle self-diffusivity. Also, inherent in the simulations is the classical description of crystal nucleation, which is qualitatively different from the description employed in the present model. The distinction between the two approaches is made evident, as discussed in previous work [12], by the different dependencies of the critical cluster size on particle volume fraction predicted by the classical and the kinetic model. Classical nucleation theory determines the critical cluster size from thermodynamic considerations so that as the supersaturation increases the critical cluster size monotonically decreases. In the present model, however, the critical cluster size is determined kinetically and is found to go through a minimum for repulsive systems (figure 5) as the particle concentration is increased. Unfortunately, the above simulations and other experiments where the critical cluster size has been measured [26] are restricted to particle concentrations much smaller than where the minimum is predicted by the kinetic model.

6. Conclusions

We have presented a kinetic model for calculating nucleation rates in charged colloidal suspensions. The charged particles are treated as effective hard spheres of enhanced sizes determined by the strength of the coulombic repulsions. A model previously developed for hard-sphere suspensions is then applied to calculate nucleation rates. Crystal nucleation and growth are determined as the result of a competition between the rates of single particle aggregation onto, and dissociation from, cluster surfaces. Developing descriptions of these processes for charged systems involves a decoupling of thermodynamic and hydrodynamic effects. The thermodynamic driving force for crystallization is determined by the effective hard-sphere volume fraction of the particles. Hydrodynamic effects are determined by the

actual volume fraction of the particles and using the excluded shell potential to represent particle interactions. Knowledge of particle aggregation and dissociation rates then allows the determination of pseudo-steady-state nucleation rates.

Intriguing trends in the dependence of the nucleation rate on the particle volume fraction are predicted as the strength and the range of particle repulsions are varied. At a fixed effective hard-sphere volume fraction, increasing either the strength or the range of particle repulsions first causes the nucleation rate to decrease below the hard-sphere value and then increase. Also, the location of the maximum in the nucleation rate observed for hard-sphere suspensions gradually shifts to higher effective volume fractions. These trends are understood using the descriptions of particle aggregation and dissociation processes developed. Preliminary comparisons indicate qualitative agreement between model predictions and experiments. Simulations on charged colloidal suspensions are in semi-quantitative agreement with model predictions. The dependence of the nucleation rate on the strength and the range of particle repulsions predicted is identical to that observed in the simulations. However, while the simulations predict nucleation rates in charged systems to be consistently larger than in hard-sphere suspensions, the model predicts otherwise. Further investigation is essential before the qualitative trends can be established.

Acknowledgments

The authors acknowledge support from the US DOE via the University of Illinois at Urbana Champaign Frederick Seitz Materials Research Laboratory grant number DEFG02-96ER45439. The authors also thank Dr F El Azhar and Dr M Baus for providing the simulation data in figure 1(b).

References

[1] Russel W B, Saville D A and Schowalter W R 1989 *Colloidal Dispersions* (Cambridge: Cambridge University Press)
[2] Monovoukas Y and Gast A P 1989 *J. Colloid Interface Sci.* **128** 533
[3] Hachisu S, Kobayashi Y and Kose A 1973 *J. Colloid Interface Sci.* **42** 342
[4] Furusawa K and Yamashita S 1982 *J. Colloid Interface Sci.* **89** 574
[5] Voegtli L P and Zukoski C F 1991 *J. Colloid Interface Sci.* **141** 92–108
[6] Voegtli L P 1989 *PhD Thesis* University of Illinois, Urbana-Champaign
[7] Robbins M O, Kremer K and Grest G S 1988 *J. Chem. Phys.* **88** 3286
[8] El Azhar F, Baus M, Ryckaert J P and Meijer E J 2000 *J. Chem. Phys.* **112** 5121
[9] Palberg T 1999 *J. Phys.: Condens. Matter* **11** R323
[10] Russel W B 1990 *Phase Transit.* **21** 127
[11] Aastuen D J W, Clark N A, Cotter L K and Ackerson B J 1986 *Phys. Rev. Lett.* **57** 1733
[12] Dixit N M and Zukoski C F 2001 *Phys. Rev.* E **64** 041604
[13] Dixit N M and Zukoski C F 2002 *Phys. Rev.* E **66** 051602
[14] Harland J L and van Megen W 1997 *Phys. Rev.* E **55** 3054
[15] Auer S and Frenkel D 2001 *Nature* **409** 1020
[16] Dhont J K G, Smits C and Lekkerkerker H N W 1992 *J. Colloid Interface Sci.* **152** 386
[17] Pusey P N and van Megen W 1987 *Complex and Supramolecular Fluids* vol 673, ed S A Safran and N A Clark
[18] Pusey P N and van Megen W 1987 *Phys. Rev. Lett.* **59** 2083
[19] Auer S and Frenkel D 2002 *J. Phys.: Condens. Matter* **14** 7667
[20] Gasser U, Weeks E R, Schofield A, Pusey P N and Weitz D A 2001 *Science* **292** 258
[21] Kang H S, Lee C S, Ree T and Ree F H 1985 *J. Chem. Phys.* **82** 414
[22] Carnahan N F and Starling K E 1969 *J. Chem. Phys.* **51** 635
[23] Hall K R 1972 *J. Chem. Phys.* **57** 2252
[24] Anderson J L, Rauh F and Morales A 1978 *J. Phys. Chem.* **82** 608
[25] Debenedetti P G 1996 *Metastable Liquids: Concepts and Principles* (Princeton, NJ: Princeton University Press)
[26] Elliot M S, Haddon S B and Poon W C K 2001 *J. Phys.: Condens. Matter* **13** L553